Icarus 212 (2011) 504–519

Contents lists available at ScienceDirect

Icarus

journal homepage: www.elsevier.com/locate/icarus

The impact of martian mesoscale winds on surface temperature and on the determination of thermal inertia

Aymeric Spiga [a,b,*], François Forget [a], Jean-Baptiste Madeleine [a], Luca Montabone [a], Stephen R. Lewis [b], Ehouarn Millour [a]

[a] Laboratoire de Météorologie Dynamique, Université Pierre et Marie Curie, Paris, France
[b] Department of Physics and Astronomy, The Open University, Milton Keynes, United Kingdom

ARTICLE INFO

Article history:
Received 17 November 2010
Revised 1 February 2011
Accepted 1 February 2011

Keywords:
Mars, Atmosphere
Mars, Surface
Atmosphere, Dynamics
Meteorology
Mineralogy

ABSTRACT

Radiative control of surface temperature is a key characteristic of the martian environment and its low-density atmosphere. Here we show through meteorological modeling that surface temperature can be far from radiative equilibrium over numerous sloping terrains on Mars, where nighttime mesoscale katabatic winds impact the surface energy budget. Katabatic circulations induce both adiabatic atmospheric heating and enhancement of downward sensible heat flux, which then becomes comparable to radiative flux and acts to warm the ground. Through this mechanism, surface temperature can increase up to 20 K. One consequence is that warm signatures of surface temperature over slopes, observed through infrared spectrometry, cannot be systematically associated with contrasts of intrinsic soil thermal inertia. Apparent thermal inertia maps retrieved thus far possibly contain wind-induced structures. Another consequence is that surface temperature observations close to sloping terrains could allow the validation of model predictions for martian katabatic winds, provided contrasts in intrinsic thermal inertia can be ruled out. The thermal impact of winds is mostly discussed in this paper in the particular cases of Olympus Mons/Lycus Sulci and Terra Meridiani but is generally significant over any sloped terrains in low thermal inertia areas. It is even general enough to apply under daytime conditions, thereby providing a possible explanation for observed afternoon surface cooling, and to ice-covered terrains, thereby providing new insights on how winds could have shaped the present surface of Mars.

1. Introduction

Regional, diurnal and seasonal variations of surface temperature are particularly large on Mars (Kieffer et al., 1976). In most cases, the low atmospheric density and heat capacity lead to negligible contributions of sensible heat flux[1] in the martian surface energy budget (Sutton et al., 1978). Consequently, the martian surface remains close to radiative equilibrium (Savijärvi and Kauhanen, 2008, their Fig. 2). This radiative control of surface temperature is a crucial component of the martian environment:

- From a geological standpoint, it allows for the unveiling of the nature and geological history of martian soils through determination of their thermophysical properties (Mellon et al., 2000; Fergason et al., 2006).
- From a meteorological standpoint, it is the central driver for intense circulations taking place at all spatial scales in the thin CO_2 martian atmosphere: large-scale thermal tides (Lewis and Barker, 2005), mesoscale anabatic/katabatic winds (Tyler et al., 2002) and microscale transitions between afternoon convective and nighttime shear-driven turbulent circulations (Spiga et al., 2010).
- From an exobiological standpoint, it imposes severe constraints on the stability of liquid water and living organisms at the martian surface (Brack, 1996).

Regional, diurnal and seasonal variations of surface temperature are dependent on the physical properties of near-surface geological materials: particle size, rock abundance, bedrock outcropping and induration (Presley and Christensen, 1997). Thermal inertia I quantifies the ability of the subsurface (e.g., top several centimeters of the soil) to absorb/store heat during the day and to (re)radiate it at night. It is defined by $I = \sqrt{k\rho c}$, with bulk thermal conductivity k, specific heat capacity c and density ρ. In martian conditions, surfaces of unconsolidated fine-grained materials tend to have low values of thermal inertia while rocky surfaces

* Corresponding author at: Laboratoire de Météorologie Dynamique, Université Pierre et Marie Curie, 75005 Paris, France.
E-mail address: aymeric.spiga@upmc.fr (A. Spiga).

[1] Sensible heat flux describes the energy exchange between the atmosphere and surface due to molecular conduction and turbulence.

0019-1035/$ - see front matter © 2011 Elsevier Inc. All rights reserved.
doi:10.1016/j.icarus.2011.02.001

and bedrock outcrops have high values (Haberle and Jakosky, 1991, their Fig. 15). *True* thermal inertia has to be inferred from *in situ* assessment of soil characteristics, which, to date, have only been possible at few locations on Mars (Hynek and Singer, 2007). Notwithstanding this, by assuming radiative control of martian surface temperature, invaluable *apparent* thermal inertia maps have been derived by comparing numerical predictions from soil thermal modeling with measurements of surface (brightness) temperature obtained by the Viking (Kieffer et al., 1977; Palluconi and Kieffer, 1981) and Mars Global Surveyor (Mellon et al., 2000; Jakosky et al., 2000; Putzig et al., 2005; Putzig and Mellon, 2007a) orbiters.

Datasets of apparent thermal inertia have become widely employed in martian geological studies, climate models, landing site selections, exobiological discussions, as a means to describe the intrinsic characteristics of martian soils. Hence it is important to discuss thoroughly possible causes of mismatch between apparent and true soil properties (e.g., Putzig and Mellon, 2007a). A key question is to what extent surface temperature contrasts can be accounted for by soil thermophysical characteristics only. The atmospheric influence on surface temperature has been acknowledged as a potentially crucial factor. Haberle and Jakosky (1991) showed how simplistic assumptions about the downward infrared flux reaching the surface in martian dusty conditions led to significant overestimates of thermal inertia, and hence soil particles' sizes. Part of the surface temperature signal carries information on atmospheric dust loading.

Dust might not be the only key atmospheric influence on martian surface temperature. The control of surface temperature on martian winds has been acknowledged in the existing literature (cf. references in the first paragraph). However, possible departures from surface radiative equilibrium caused by atmospheric circulations have either been overlooked or considered as second-order corrections (Ye et al., 1990). Recently, Spiga and Forget (2009) suggested through three-dimensional mesoscale modeling that nighttime katabatic winds could warm the slopes of Olympus Mons up to 20 K compared to surrounding terrains, forming a "warm katabatic ring" at the base of the volcano. This finding deserved to be examined in more detail than in the brief preliminary discussions of Spiga and Forget (2009, Section 4.6). In this paper, we describe both the impact of mesoscale winds on martian surface temperature and the key implications of this phenomenon, particularly on thermal inertia retrievals. The main purpose is to show how surface radiative equilibrium – an assumption central to many martian studies – does not hold in numerous martian sloping terrains.

The paper is organized as follows. In Section 2, we describe observations of nighttime surface warming in the Olympus Mons region. In Section 3, we explain why those observations have been related to contrasts in thermal inertia until now. In Section 4, we detail our new explanation based on mesoscale winds and determine how those can impact the martian surface energy budget. Consequences on thermal inertia retrievals are discussed in Section 5. In Section 6, we describe why Olympus Mons is only one example amongst others. In Section 7, we briefly exploit the general character of our conclusions to discuss daytime conditions and ice-covered slopes. We summarize our results in Section 8.

2. Observations of nighttime surface warming

Spiga and Forget (2009) identified the nighttime "warm katabatic ring" at the base of Olympus Mons through mesoscale modeling (cf. Fig. 13 of that paper). This phenomenon can also be identified in remote-sensing surface temperature measurements. Fig. 1 shows composite maps of surface temperature remotely sounded around local time 02:00 by the Thermal Emission Spectrometer (TES) on board Mars Global Surveyor (MGS) during three martian years (Christensen et al., 2001; Smith et al., 2001). In order to avoid situations where surface temperature retrievals are impacted by airborne dust (Haberle and Jakosky, 1991), nighttime maps in Fig. 1 are generated by spanning intervals of areocentric solar longitude[2] during non-dusty seasons when infrared dust opacity is lower than 0.2 and undergoes only moderate temporal variations.

Significant surface temperature enhancements are observed by TES at the base of Olympus Mons compared to surrounding plains (for reference, Fig. 2 shows the volcano's topography and slope angles). Numerous non-dusty L_s intervals other than Fig. 1's have been tested and always show the nighttime "warm katabatic ring" on Olympus slopes (figures not displayed for the sake of brevity). This is true for all martian years monitored by TES. The difference of surface temperature between surrounding terrains and the slopes of Olympus Mons is over +10 K (except for the less steep northeastern slope) and reaches +20 K in specific locations. Temperature contrasts between slopes and plains in the Olympus region have similar amplitudes whichever season or martian year is considered. A closer look at TES observations shows that not only the immediate slopes of Olympus Mons are impacted but also topographical ridges in surrounding terrains (e.g., Lycus Sulci), westward of the topographical obstacle. Note that no adverse influence of sloping terrains on TES temperature measurements is reported in the literature (e.g., Christensen et al., 2001) as far as nighttime observations are concerned (Putzig and Mellon, 2007b, discuss the issue for daytime observations). TES measurements were carried out at a narrow range of local times at night (near 02:00 at all but polar latitudes), thus it is not possible to infer the local time at which the Olympus Mons nocturnal "warm katabatic ring" appears. Nevertheless, this could be estimated through Mars Express observations: while no surface warming at the base of Olympus Mons is detected by the Planetary Fourier Spectrometer (PFS) around local time 20:00 (Wolkenberg et al., 2010),[3] recent infrared measurements by the OMEGA spectrometer indicate the presence of the "warm katabatic ring" around local time 22:30 (B. Gondet and Y. Langevin, personal communication).

TES measurements provide observational evidence for the nighttime "warm katabatic ring" phenomenon on Olympus Mons slopes. The remaining question is then: what causes this observed phenomenon to exist on the martian surface? Two scenarios can be proposed. On the one hand, warm signatures on slopes could be caused by systematic contrasts of soil thermophysical properties: it is the interpretation implicitly adopted to date in thermal inertia retrievals. On the other hand, as preliminarily assessed in Spiga and Forget (2009), those signatures could be caused by atmospheric winds. It is the second interpretation that this paper seeks to establish.

3. Interpretation in terms of thermal inertia structures

3.1. Scenario

The scarcity of martian *in situ* missions only allows for evaluating true thermal inertia at few locations on the planet, although the two mobile Mars Exploration Rovers (MER) have significantly extended the existing coverage (Hynek and Singer, 2007). Instead, apparent thermal inertia is derived from orbital measurements of

[2] The areocentric solar longitude L_s is an angular quantity between 0° and 360° that defines the position of Mars on its orbit around the Sun. $L_s = 0°$ is defined as the northern spring equinox.

[3] Discussions in Wolkenberg et al. (2010) on PFS observations mostly focus on daytime atmospheric warming in Tharsis/Olympus terrains. Also termed a "warm ring", it is a completely different effect than the "warm katabatic ring" discussed in this paper.

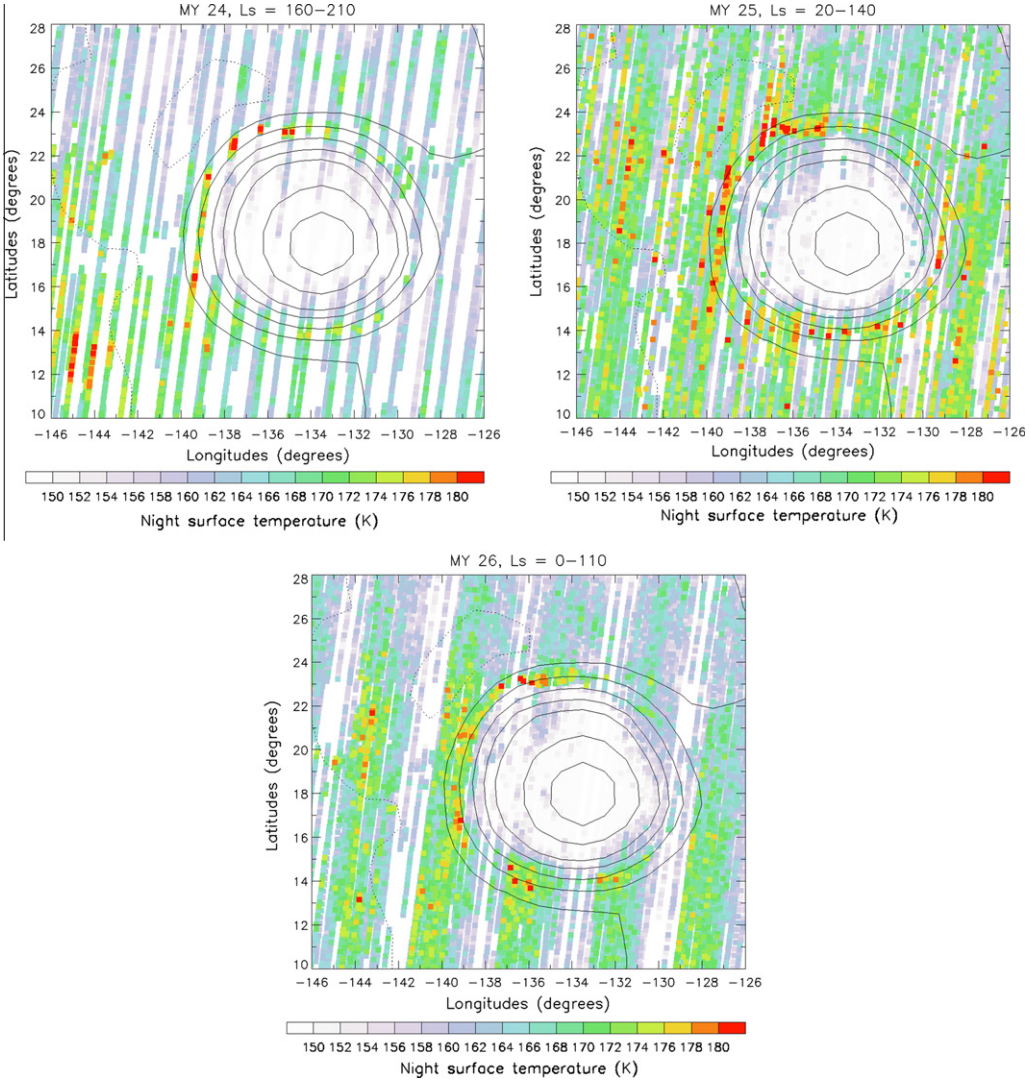

Fig. 1. Surface temperature (K) remotely sounded by MGS-TES around local time 02:00 in the Olympus Mons/Lycus Sulci area for Martian Year 24, 25 and 26 (according to numbering proposed in Clancy et al. (2000)). Topography is contoured (contour interval is 3 km).

surface temperature (e.g. with TES Mellon et al., 2000; Jakosky et al., 2000; Putzig et al., 2005, 2007a). The principle is to consider thermal inertia as a free input parameter for soil thermal modeling and calculate values for which modeled surface temperature best fit observations. The methodology depends in practice on the availability of data with local time. The best accuracy is obtained when fitting the whole observed daily cycle of surface temperature. Most missions to Mars have used near-polar or Sun-synchronous orbits thus severely limiting the local time sampling of a given region. For instance, only one daytime/nighttime TES surface temperature value is available each sol for a given martian site. Thus, maps of apparent thermal inertia are more often derived with the help of look-up tables generated from soil thermal modeling (Mellon et al., 2000).

Numerical soil modeling generally treats the thermal behavior of the martian surface as an upper boundary condition on the heat diffusion equation (e.g., Putzig and Mellon, 2007a). In nighttime conditions, assuming seasonal CO_2 condensation does not occur,[4] upward longwave radiative loss is nearly balanced by subsurface heat conduction and downwelling longwave radiation due to both atmospheric CO_2 and aerosols, hence the simplified equation for surface energy budget

$$\epsilon\sigma T_s^4 = I\sqrt{\frac{\pi}{\tau}}\left.\frac{\partial T_g}{\partial \zeta}\right|_{\zeta=0} + \mathcal{F}_{IR} \quad (1)$$

with thermal inertia I as defined in the introduction, surface emissivity ϵ, Stefan–Boltzmann constant σ, surface temperature T_s, downward infrared flux $\mathcal{F}_{IR}$, diurnal period of thermal wave τ, temperature in the ground T_g at depth ζ.

Using Eq. (1) in soil thermal modeling for thermal inertia retrievals relies on the assumption that, in the thin martian atmosphere, sensible heat flux plays a minor role in the martian surface energy budget. In other words, Eq. (1) describes the martian surface at radiative equilibrium and implies that, in non-dusty conditions, spatial structures in surface temperature are caused by spatial contrasts of soil thermophysical properties.[5] The surface is warmer at night where the ground is able to retain heat stored dur-

[4] For thermal inertia retrievals in polar regions, a term relative to CO_2 condensation must be included. For the sake of simplicity, we omit it in the discussion as we consider low- and mid-latitude terrains. See Section 7.2 for discussions in polar regions.

[5] Note that we exclude the potential influence of buried subsurface ice in high latitudes (Bandfield and Feldman, 2008) and on mid-latitude pole-facing slopes (Vincendon et al., 2010).

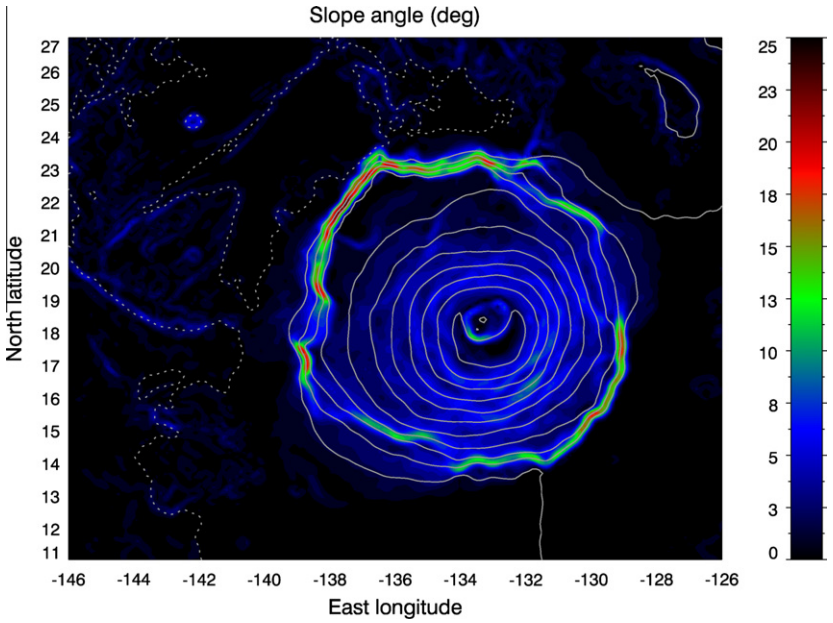

Fig. 2. Local slope angle (°) calculated from Mars Orbiter Laser Altimeter topography interpolated on the grid defined for mesoscale simulation in Section 4.1 (6 km grid spacing). Maximum value is ~30°. Topography is contoured (contour interval is 2 km).

ing the day for a longer time. Thus, in the hypothetical scenario where Eq. (1) holds, the Olympus Mons nocturnal "warm katabatic ring" identified in Fig. 1 posits a similar structure of high thermal inertia at the base of the volcano, correlated with slope steepness (cf. Fig. 2 and discussions in Section 5). This is indeed the case in the Putzig and Mellon (2007a) state-of-the-art TES thermal inertia retrievals shown in Fig. 3. Thermal inertia is between three to five times higher at the base of Olympus Mons than on surrounding terrains. This is also true for Lycus Sulci slopes westward of Olympus Mons. High values of thermal inertia on the Olympus Mons slopes can also be distinguished in Fig. 8 (nighttime map) of Putzig and Mellon (2007a).

3.2. Discussion

Could the martian soil on Olympus slopes have a different geological nature causing high thermal inertia signatures, apparently correlated with slope steepness? We do not attempt to provide a complete answer to this issue, clearly out of the scope and expertise of this paper. However, we detail a few problems with interpreting surface temperature signatures on Olympus slopes in terms of intrinsic thermal inertia contrasts.

Firstly, nighttime and daytime thermal inertia maps are very different in the vicinity of terrains such as Olympus Mons (Putzig and Mellon, 2007a, their Fig. 8). Notably, there is no "ring" of

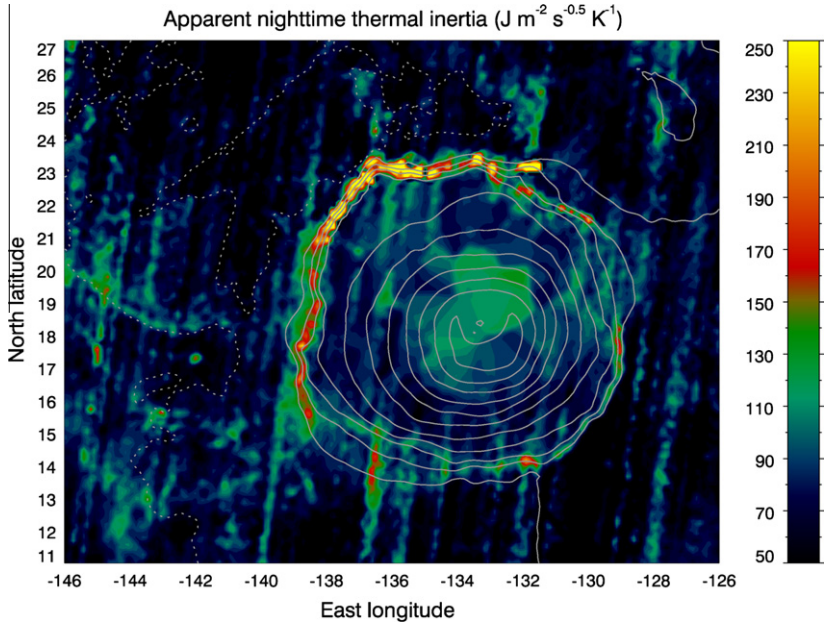

Fig. 3. Nighttime apparent thermal inertia (J m^{-2} $s^{-1/2}$ K^{-1}) retrieved by Putzig and Mellon (2007a) from TES surface temperature measurements in the Olympus Mons/Lycus Sulci area. Topography is contoured (contour interval is 2 km).

higher thermal inertia at the base of the volcano in daytime maps. Amongst numerous potential reasons, those differences might indicate that retrieved structures of thermal inertia near volcanoes are not related to the intrinsic nature and properties of the soil (otherwise daytime/nighttime computations would converge) but to phenomena not taken into account in the retrievals.

Secondly, despite much effort and the use of sophisticated techniques (Putzig et al., 2005; Putzig and Mellon, 2007a), "stripes" of thermal inertia correlated with orbital trajectories cannot be avoided in the maps (Fig. 8 of Putzig and Mellon (2007a)). There may be many reasons for such spurious structures to appear, but one of them is that the assumption about surface temperature and thermal inertia being closely linked through soil radiative equilibrium is invalid in certain regions. As we suggest in the following sections, Eq. (1) might not be a relevant model for thermal inertia retrievals over martian sloping terrains.

Thirdly, high thermal inertia signatures are correlated with the steepest slopes of Olympus Mons, while values of thermal inertia for both its summit and base plains are similar. Olympus slopes are considered part of the large basaltic shield volcano shaped by lava flow (Bleacher et al., 2007) while plains below its flanks exhibit complex geological structures, giving insights into recent fluvial, volcanic, tectonic activity (Basilevsky et al., 2006). Why then would the flanks of Olympus Mons have peculiarly different soil thermophysical properties than both summit and plains? Processes that shaped the asymmetrical flanks remain an active topic of research (McGovern and Morgan, 2009), but still one would not expect thermal inertia signatures to remain confined to slopes given downslope volcanic spreading. The fact that Lycus Sulci slopes display high thermal inertia patterns also needs to be accounted for.

4. New interpretation in terms of wind-induced phenomena

We propose an alternative explanation to thermal inertia contrasts to account for surface temperature enhancements monitored by TES on Olympus Mons slopes (Fig. 1). Instead of the spatial variations of soil thermophysical properties, our scenario involves mesoscale atmospheric winds over martian slopes. We show that those winds could have a strong thermal impact both on atmosphere and surface.

4.1. Mesoscale modeling

"Mesoscale" refers to atmospheric circulations which develop over horizontal scales of less than 100 km. High-resolution modeling strategies are necessary to resolve those circulations. We use the martian mesoscale model built at Laboratoire de Météorologie Dynamique and described in details in Spiga and Forget (2009). This model resolves three-dimensional fluctuations of atmospheric winds, temperature and pressure in a particular region of Mars down to few kilometers resolution. It couples a new-generation fully compressible non-hydrostatic terrestrial solver (Weather Research and Forecast (WRF), see Skamarock and Klemp, 2008), adapted to Mars, with state-of-the-art martian physical parameterizations developed for Mars global climate modeling (GCM, see Forget et al., 1999), and additional schemes suitable for mesoscale applications (e.g., a parameterization for slope irradiance effects, Spiga and Forget, 2008). The model includes treatment of CO_2 and dust radiative transfer, boundary-layer mixing by sub-grid scale turbulent processes and, of particular interest for the present study, computations of soil thermal conduction through a 10-layer model described in Hourdin et al. (1993). Surface temperature computed in the general circulation model has been validated against MGS-TES (Millour et al., 2008) and Mars Express/OMEGA (Jouglet et al., 2009) measurements averaged over a GCM grid box. Initial and boundary conditions needed for limited-area mesoscale computations with the Spiga and Forget (2009) model are extracted from simulations with the Forget et al. (1999) GCM which shares similar physical parameterizations, hence reducing relevant inconsistencies. Both models use a "dust scenario" prescribed from MGS measurements in Martian Year 24 and 25 and thought to be representative of martian atmospheric conditions outside of planet-encircling dust storm events (cf. Section 2.3.3 in Spiga and Forget (2009)).

Mesoscale simulations using a horizontal grid spacing of 6 km are carried out in a domain centered on Olympus Mons with an uniform soil thermal inertia of 85 $J\,m^{-2}\,s^{-1/2}\,K^{-1}$, which is the average thermal inertia for plains surrounding the volcano (according to the dataset of Putzig and Mellon (2007a)). Spatial structures of thermal inertia around Olympus Mons in Fig. 3 are therefore prevented from influencing surface temperature, which allows us to unambiguously identify the impact of mesoscale winds on surface temperature.

Surface temperature simulated by the LMD mesoscale model is shown in Fig. 4 for northern fall equinox and Fig. 5 for northern summer, at the same local time as TES surface temperature measurements in Fig. 1. Mesoscale modeling reproduces the nighttime "warm katabatic ring" at the base of Olympus Mons. Absolute values of surface temperature in northern summer and fall, as well as relative contrasts between Olympus slopes and surrounding plains, are in qualitative and quantitative agreement with TES retrievals shown in Fig. 1. A maximum surface temperature of 180 K is both observed by TES, and simulated[6] by the LMD mesoscale model under the assumption of uniform thermal inertia. As is the case in TES data, the steepest flanks on the northern and western side of Olympus Mons (cf. Fig. 2) are prone to the strongest surface warming, reaching +20 K compared to the surrounding plains, while southern and eastern flanks are less impacted (except for the southeastern corner). The steepest slopes of Lycus Sulci terrains westward and northward of Olympus are also subject to surface warming. As it is shown in Fig. 6, simulations with different horizontal resolution of 10 and 20 km yield similar qualitative and quantitative results as Fig. 4, as long as the topographic slopes are resolved with enough accuracy.

Thus, physically-consistent mesoscale modeling shows that nighttime surface warming over slopes might occur without soil thermal properties being necessarily involved. Meteorological simulations point out significant atmospheric contributions to Eq. (1) not taken into account in soil thermal modeling used to retrieve thermal inertia from surface temperature measurements. As a result, as far as structures over Olympus Mons and Lycus Sulci slopes are concerned, surface temperature maps from mesoscale predictions (Figs. 4–6) and apparent thermal inertia maps from soil modeling (Fig. 3) are strikingly similar. How do atmospheric circulations lead the martian surface to warm at night over steep slopes? Diagnostics from mesoscale modeling can help to answer this question.

4.2. Role of katabatic winds

4.2.1. Adiabatic warming of atmosphere

In nighttime conditions over Olympus Mons, radiative cooling occurs at the surface and temperature inversions take place in

[6] Subtle seasonal differences of nighttime surface temperature (~2–3 K) can be noticed through a careful comparison of Figs. 4 and 5 (such differences can be found in TES measurements too). Nevertheless, the characteristics of the nighttime "warm katabatic ring" are similar in those two mesoscale simulations and, more generally, in mesoscale simulations performed at various non-dusty seasons (not shown here for brevity).

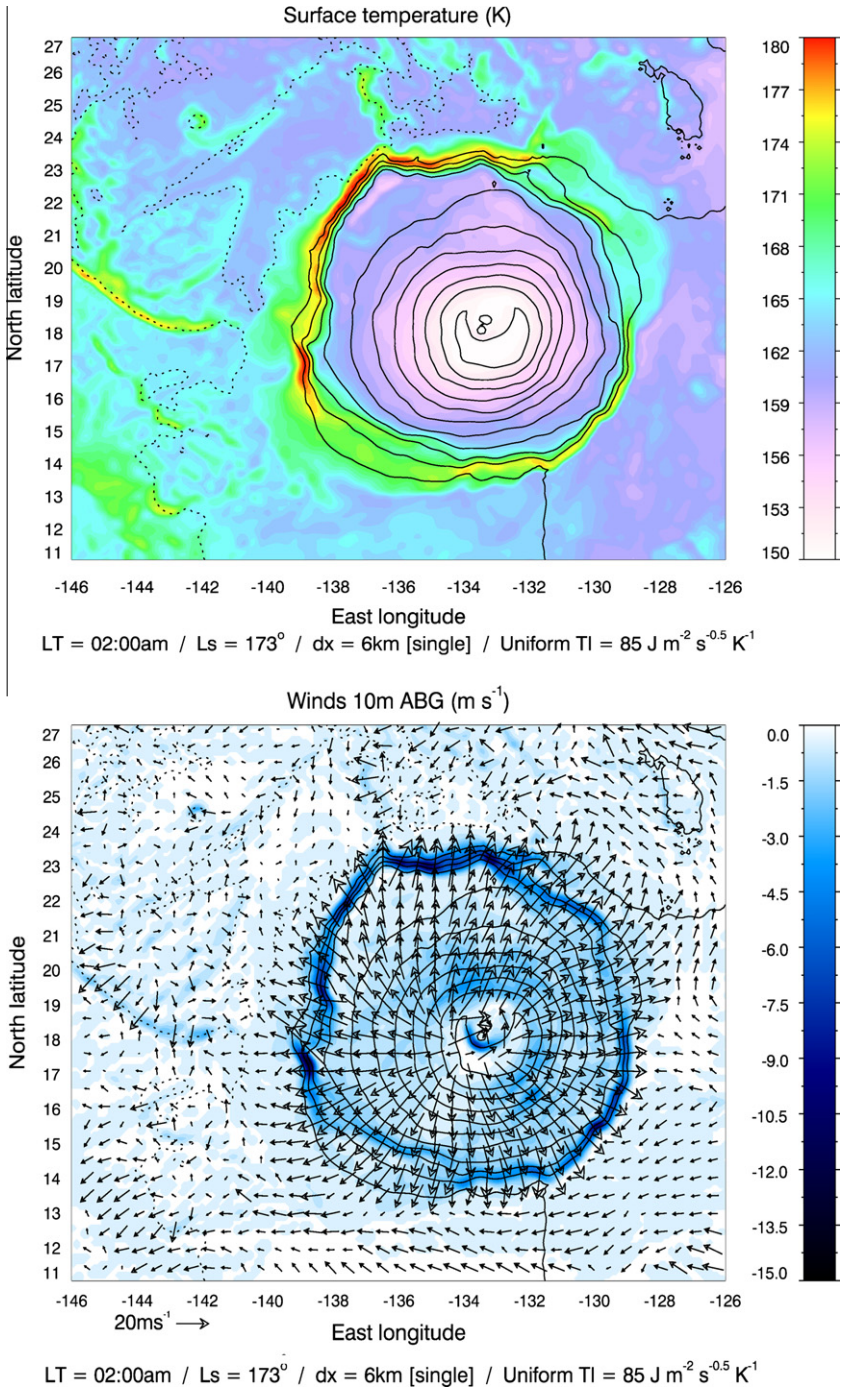

Fig. 4. Surface temperature (K, top) and winds 10 m above local surface (m s^{-1}, bottom) predicted in the Olympus Mons/Lycus Sulci area by a mesoscale simulation using the Spiga and Forget (2009) model with 6 km horizontal resolution and assuming uniform soil thermal inertia of 85 J m^{-2} $s^{-1/2}$ K^{-1}. Note that the simulation domain is larger than the area displayed in this figure. Season is northern fall, local time 02:00. Topography is contoured (contour interval is 2 km). In the bottom plot, vectors (plotted for every 5th grid point) indicate wind direction with vector length being proportional to horizontal wind speed; vertical wind velocity is shaded (it is positive for upward atmospheric circulations).

the near-surface atmosphere, then warmer than the surface. Numerous studies in the terrestrial and martian literature described how downslope (so-called katabatic) circulations develop close to topographical obstacles and over gently-sloping plains (Ye et al., 1990; Savijärvi and Siili, 1993; Tyler et al., 2002; Rafkin and Michaels, 2003; Spiga and Forget, 2009; Savijärvi and Määttänen, 2010), while cool dense air is accelerated down sloping terrains by gravity, overcoming the opposing downslope pressure gradient. Katabatic acceleration increases with slope steepness for a given temperature inversion (Spiga, 2011, Eq. (2)). Strong near-surface inversions yield martian katabatic wind magnitudes that are two to three times greater than on Earth despite the much lower gravity on the Red Planet. Fig. 4 shows that the nighttime regime of mesoscale wind in the vicinity of Olympus Mons is dominated by katabatic flow. The largest surface temperature enhancements are observed on the steepest slopes (cf. Fig. 2), where the vertical wind component is maximized. The prominence of steady katabatic flow in mesoscale wind regime over uneven topographical terrains such as Olympus Mons is observed all night long and for various seasons.

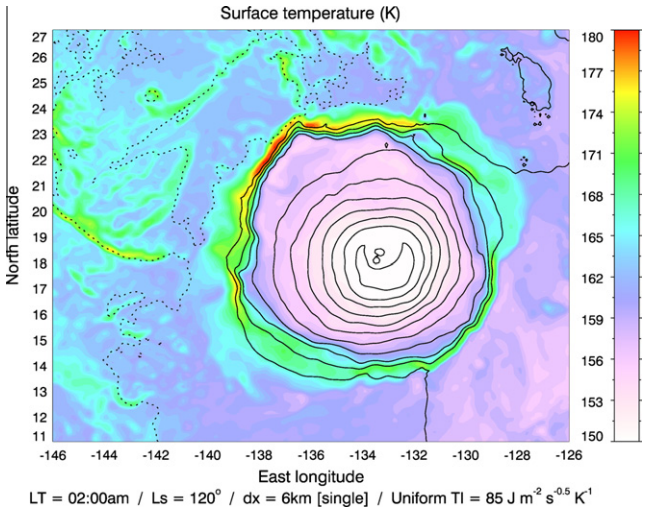

Fig. 5. Surface temperature (K) as in Fig. 4 top, except that mesoscale simulations are run in northern summer ($L_s = 120°$).

What is the impact of martian katabatic winds on atmospheric temperature? Fig. 7 shows temperature and wind profiles in the near-surface atmospheric layer above two locations at the same longitude, one over Olympus flanks and one over surrounding flat plains. Over the flanks of Olympus Mons, the vertical profiles of temperature and wind indicate to first order Prandtl-like slope wind regime, arising from quasi-equilibrium between katabatic acceleration and near-surface friction (e.g. Mahrt, 1982; Savijärvi and Siili, 1993). The katabatic wind layer extends up to 1 km above the surface over the Olympus slope, with horizontal component reaching 38 m s^{-1} and vertical component reaching 14 m s^{-1}.

Those orders-of-magnitude for near-surface katabatic winds are not uncommon on Mars, especially in the vicinity of the steep slopes of martian volcanoes, craters and canyons, as shown by previous mesoscale modeling studies (Rafkin and Michaels, 2003). Notably, predictions of Valles Marineris and Olympus Mons slope winds from other model runs show satisfactory agreement with amplitudes above 30 m s^{-1} (Spiga and Forget, 2009, Sections 3.3 and 3.5). Note that mesoscale models have only been validated in plains where Viking and Pathfinder landers acquired near-surface measurements (Rafkin et al., 2001; Tyler et al., 2002; Toigo and Richardson, 2002; Spiga and Forget, 2009) but not in the most uneven martian terrains. However, those numerical models correctly replicate slope wind-related phenomena observed from orbit such as dust spiral clouds (Rafkin et al., 2002), water ice clouds associated with topography (Michaels et al., 2006; Spiga and Forget, 2009) and orientation of aeolian surface features such as streaks (Greeley et al., 2003). All these elements suggest that mesoscale modeling offers robust-enough predictions for martian slope winds.

In Fig. 7, the nighttime near-surface circulation close to slopes greatly contrasts with conditions in flat plains, where vertical wind is negligible and horizontal wind magnitude is below 5 m s^{-1} up to 500 m above the local surface. This contrast in wind regime between volcano flanks and the surrounding plains leads to contrasts in temperature. According to Fig. 7, greater atmospheric temperatures are predicted over slopes than over plains up to 1000 m above the local surface. Differences in atmospheric temperature between the two considered points (+25 K) are greater than that of surface temperature (+18 K) up to 200 m above the local surface. Diagnostics shown in Fig. 7 at one particular location are valid all around Olympus Mons as atmospheric warming is correlated with maxima of near-surface wind magnitude (see Fig. 13 (right) in Spiga and Forget (2009)). This correlation has a direct physical cause. Adiabatic compression of air, and thereby atmospheric warming, is caused by intense downward (katabatic) motions over slopes. Similar phenomena occur in terrestrial polar regions prone to strong katabatic currents. Through *in situ* meteorological measurements, Nylen et al. (2004) have reported clear-cut 30 K atmospheric warming during a strong katabatic event in the McMurdo Dry Valleys in Antarctica.

In the absence of significant nighttime diabatic heating, adiabatic warming by downslope motions is the most plausible explanation for larger near-surface atmospheric temperatures above slopes. It is also quantitatively prominent. The heating rate of an atmospheric parcel with vertical wind velocity w is given by

$$\mathcal{J}_{\text{adiab}} = -\frac{g}{c_p} w \tag{2}$$

where g is the acceleration of gravity and c_p the atmospheric specific heat capacity.[7] About 10 m above the Olympus Mons northeastern flank considered in Fig. 7, the vertical component of the wind is $w \sim -13$ m s^{-1} hence adiabatic heating rate $\mathcal{J}_{\text{adiab}} \sim 0.06$ K s^{-1}. Typical values of longwave cooling rate predicted at this altitude through radiative transfer calculations in the mesoscale model are ~0.001–0.003 K s^{-1}, i.e. an order-of-magnitude lower. Warming induced by adiabatic compression through vertical motion is not balanced by infrared radiative cooling, hence the much warmer atmosphere over slopes than over plains.

4.2.2. Enhancement of sensible heat flux

It remains to be explained why a warmer atmosphere yields a warmer surface, particularly above the steepest slopes of the Olympus volcano and Lycus Sulci terrains. In their preliminary discussions, Spiga and Forget (2009) and Spiga et al. (2010) proposed that *surface temperature increases as the warmer overlying atmosphere enhances the downward infrared flux to the surface*. Although the physics behind this statement is correct (see e.g. Savijärvi et al., 2004), further analysis shows that the amplitudes of downward infrared flux are insufficient to account for a 20 K increase at the base of Olympus Mons. As shown in Fig. 8, where atmospheric heating through katabatic circulation occurs, downward longwave flux is only enhanced of about 3–4 W m^{-2} compared to other terrains. Such radiative departures are unlikely to induce the observed and simulated enhancements of surface temperature at the base of Olympus Mons.

The contrasts of sensible heat flux caused by mesoscale atmospheric motions over slopes are more likely to cause the Olympus nighttime "warm katabatic ring". Fig. 8 shows predicted values for sensible heat flux in the mesoscale model (downward flux is positive since the atmosphere is warming the surface at night). Sensible heat exchanges are more than one order of magnitude larger (~30 W m^{-2}) above Olympus Mons slopes than in the surrounding terrains (~1–3 W m^{-2}), where sensible heat flux is close to values measured by Viking landers at night (Sutton et al., 1978). Furthermore, maxima of modeled sensible heat flux correlate with maxima of both surface temperature (Fig. 4) and apparent thermal inertia (Fig. 3) in Olympus Mons and Lycus Sulci.

Our simulation shows that, despite the low density of the martian atmosphere, sensible heat flux cannot be systematically neglected in the surface energy budget. Surface radiative equilibrium does not hold over most Olympus Mons slopes, where sensible heat flux is comparable to longwave radiative loss

[7] According to hydrostatic equilibrium, an atmospheric parcel with vertical wind velocity w and temperature T undergoes an increase in pressure p such as $Dp/Dt = -\frac{p}{RT} gw$ [equation A] with lagrangian derivative D/Dt and ideal gas constant R. In an adiabatic motion, such as katabatic winds, the potential temperature $\theta = Tp^{-R/c_p}$ of a particle is conserved: $D\theta/Dt = 0$ [equation B]. Combining equations A and B yields particle heating rate $\mathcal{J}_{\text{adiab}} = DT/Dt = -gw/c_p$.

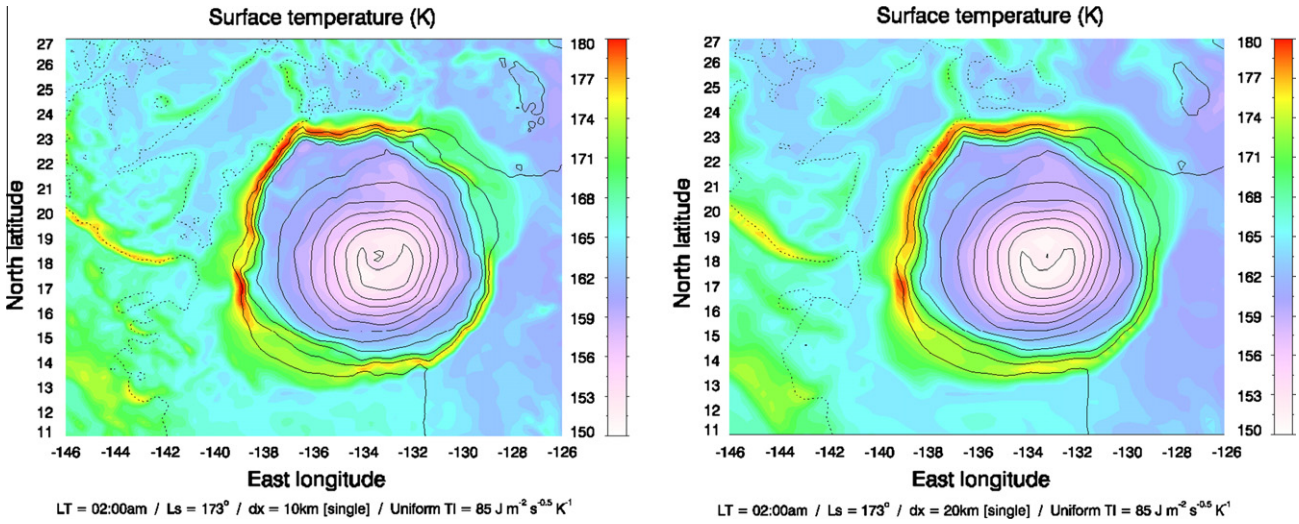

Fig. 6. Surface temperature (K) as in Fig. 4 top, except that mesoscale simulations are run with horizontal resolutions of 10 km (left) and 20 km (right).

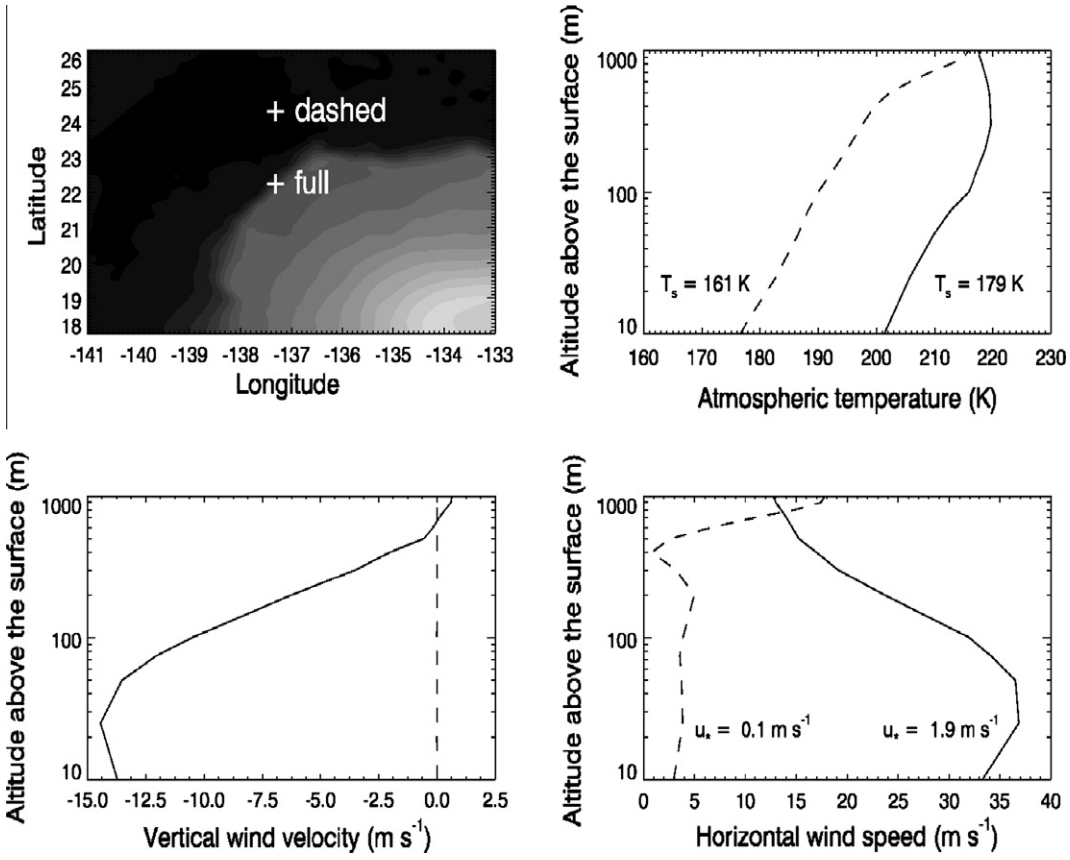

Fig. 7. Vertical profiles of near-surface temperature (K, top right), vertical wind velocity (m s^{-1}, bottom left) and horizontal wind speed (m s^{-1}, bottom right) at two particular grid points of the mesoscale simulation described in Fig. 4. As shown in the top left map, the profiles are extracted over the northwestern flank of Olympus Mons (full lines) and over the plain northward of Olympus Mons (dashed lines). The values of surface temperature and friction velocity are provided on the relevant panels of the figure.

($\sim$30 W m^{-2}). Martian surface temperature is impacted by the presence of an atmosphere in motion, especially over sloping terrains. Eq. (1) should be replaced by

$$\epsilon\sigma T_s^4 = I\sqrt{\frac{\pi}{\tau}}\frac{\partial T_g}{\partial\zeta}\Big|_{\zeta=0} + \mathcal{F}_{IR} - H_s \quad (3)$$

where H_s is the sensible heat flux.

The key factor is the enhancement of sensible heat flux by intense downslope katabatic winds, which allows for atmospheric warming by adiabatic processes to play a role in warming the surface. In other words, katabatic winds are an efficient way to cause near-surface mixing in nighttime stable conditions where buoyant turbulence/convection could not exist. This is the nighttime (more extreme) counterpart of one of Ye et al.'s (1990) conclusions for daytime upslope winds: *unlike the Earth, sensible surface heat fluxes*

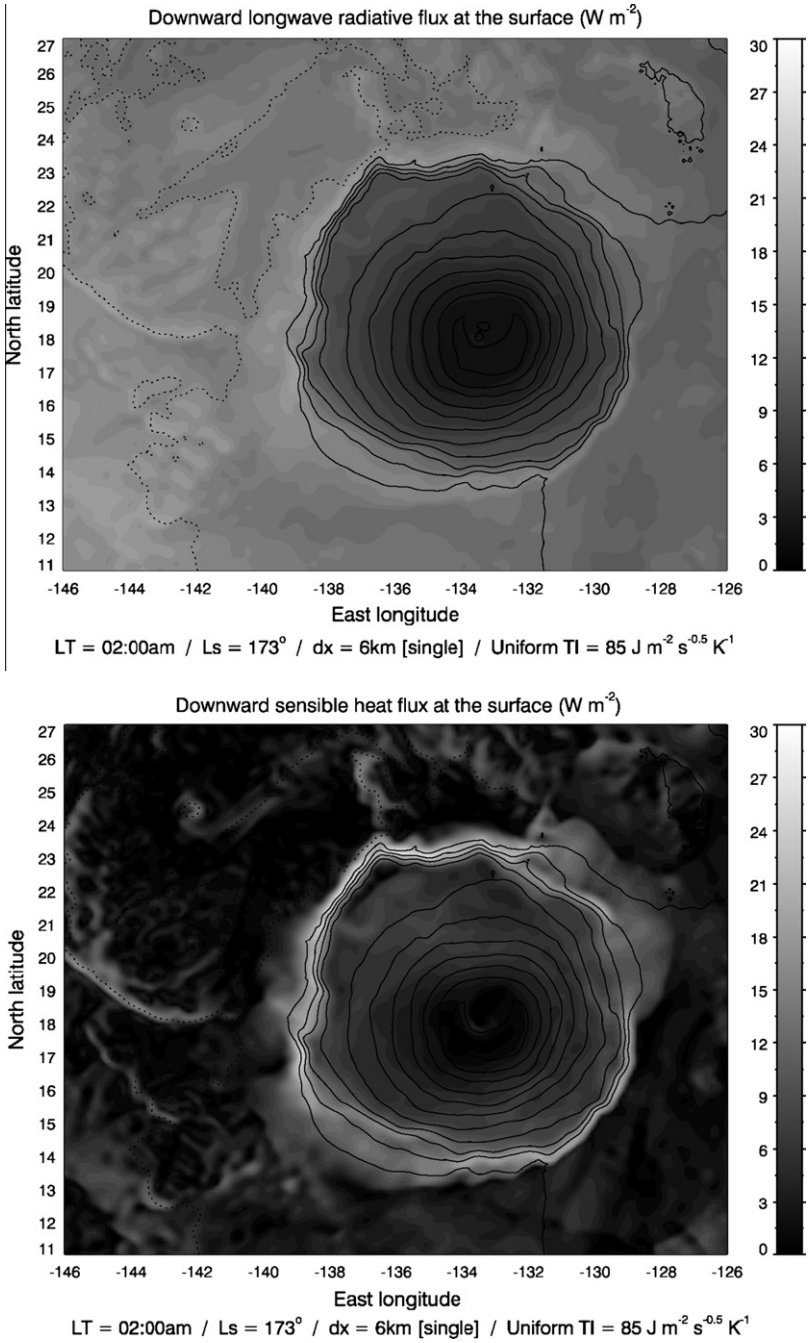

Fig. 8. Downward longwave radiative flux (W m^{-2}, top) and downward sensible heat flux (W m^{-2}, bottom) at the surface predicted in the Olympus Mons/Lycus Sulci area by the mesoscale simulation described in Fig. 4. Topography is contoured (contour interval is 2 km). Note that downward sensible heat flux corresponds to $-H_s$ according to the convention adopted in this paper: sensible heat exchanges act to warm the surface in the white areas of the bottom plot.

on Mars are noticeably dependent on the intensity of surface wind speed. To clarify this in our Olympus Mons case study, simple estimates of sensible heat flux H_s can be made through the bulk aerodynamic formula $H_s = \rho c_p \sqrt{C_d} u_* T_*$ where $T_* = T_s - T(z_1)$ is the temperature difference[8] between surface and atmosphere at altitude z_1 above ground, $C_d = [0.4/\ln(z_1/z_0)]^2$ is the von Karman neutral drag coefficient with surface roughness $z_0 = 1$ cm for martian applications, and $u_* = \sqrt{C_d} V(z_1)$ is the friction velocity with $V(z_1)$ the horizontal wind speed at altitude z_1. This formula is used in boundary layer parameterizations in the mesoscale model to represent surface–atmosphere interactions (see Appendix A). According to predictions in Fig. 7, what makes sensible heat flux being close to -30 W m^{-2} above Olympus slopes while it is -2 W m^{-2} above surrounding plains is predominantly the much higher wind speed (u_* peaks at 1.9 m s^{-1} vs. 0.1 m s^{-1}) rather than the improved thermal contrast between atmosphere and surface. A sensible heating rate $\mathcal{J}_{\text{sensible}}$ can be estimated by vertical derivative of H_s (divided by $\rho\ c_p$, cf. heat diffusion equation). Within the Olympus slope wind layer, we then have approximately $\mathcal{J}_{\text{sensible}} \sim -C_d V(z_1) \partial T/\partial z \sim -6 \times 10^{-2}$ K s^{-1}. Interestingly, the orders of magnitude of $\mathcal{J}_{\text{adiab}}$

[8] Sensible heat flux is positive if surface is transferring energy to atmosphere. The exact formula for bulk aerodynamic parameterization (the one used in the mesoscale model) makes use of potential temperature instead of temperature. In discussions we substituted temperature for potential temperature for the sake of simplicity; respective values for T_* are very close in near-surface atmospheric layers.

and $\mathcal{J}_{\text{sensible}}$ are similar: the intense instantaneous adiabatic heating rate ($0.06\ \text{K s}^{-1} = 222\ \text{K h}^{-1}$) is compensated by equally strong turbulent cooling. Sensible heat flux is an efficient way to communicate to the surface the atmospheric adiabatic heating caused by downslope katabatic wind.[9]

5. Consequences on thermal inertia retrievals

What is the impact on thermal inertia retrievals of neglecting atmospheric contributions in soil thermal modeling? The warm surface departures at night observed from orbit on Olympus slopes might be accounted for by katabatic winds only, without spatial contrasts of thermal inertia being involved. Attributing most surface temperature variations to thermal inertia[10] could cause significant artifacts in apparent thermal inertia. This is suggested by striking similarities between Figs. 3 and 4. Further quantitative insights are now obtained.

Fig. 9 shows the annual mean, maximum and minimum values of surface temperature computed through single-column modeling sharing similar schemes for radiative transfer, soil energy budget, boundary-layer mixing as mesoscale simulations. All other parameters being equal (and corresponding to Olympus conditions of Fig. 4), surface temperatures at local time 02:00 have been calculated for distinct values of thermal inertia. Fig. 9 shows that a nighttime 20 K enhancement of surface temperature exceeds by about a factor of 2 the maximum amplitude of seasonal variations. The impact of this enhancement on apparent thermal inertia is particularly strong in the range 160–180 K.

The rationale for the single-column approach is to obtain a simple link between surface temperature and thermal inertia according to Eq. (1), while excluding the control of atmospheric dynamics on surface temperature. We do not aim to compute thermal inertia as accurately as in the literature (Mellon et al., 2000; Putzig and Mellon, 2007a), but to determine relative departures (or artifacts) of thermal inertia caused by mesoscale atmospheric winds. We use surface temperature in Olympus terrains predicted through mesoscale modeling (Fig. 4) to retrieve apparent thermal inertia, as if model results were remotely sounded through orbiting spectrometry without knowing that the only cause of temperature contrasts is atmospheric dynamics. Fig. 10 is similar to Fig. 9 except it is computed specifically at $L_s = 173°$ so as to generate a map of "wind-induced" apparent thermal inertia from Fig. 4. Variations of surface temperature T_s with soil thermal inertia I are found to be reasonably represented by $T_s = a_0(a_1 - e^{-a_2 I})$ with $a_0 = 64.83$ K, $a_1 = 3.15$ and $a_2 = 5.45 \times 10^{-3}\ \text{J}^{-1}\ \text{m}^2\ \text{K}\ \text{s}^{1/2}$ in the range $I \leqslant 400\ \text{J m}^{-2}\ \text{K}^{-1}\ \text{s}^{-1/2}$. Apparent thermal inertia can be derived from surface temperature through $I = -a_2^{-1}\ln(a_1 - a_0^{-1}T_s)$.

Fig. 11 shows the application of this simple function $I = f(T_s)$ to surface temperature T_s predicted by mesoscale simulations assuming uniform thermal inertia (cf. Fig. 4). Wind-induced thermal inertia field in Fig. 11 and actual retrievals in Fig. 3 appears in striking similarity both qualitatively and quantitatively. Thermal inertia structures correlates well with Olympus slopes, with higher values where slope is steeper (compare Fig. 11 with Fig. 2). This is also true in the surrounding Lycus Sulci terrains featuring more moderate slopes. Apparent thermal inertia does not peak as high over Olympus slopes in the mesoscale predictions as in the actual retrievals. Yet most contrasts are accounted for: temperature differences caused by atmospheric motions in sloping terrains can explain the thermal inertia difference of a factors 2–5 between slopes and plains in the Olympus region. Starting from an uniform thermal inertia, we are able through mesoscale simulations to reproduce a map of apparent thermal inertia satisfyingly close to what is retrieved from orbit. Most retrieved thermal inertia structures around Olympus Mons can be as well interpreted as wind-induced structures as actual variations of intrinsic soil properties.

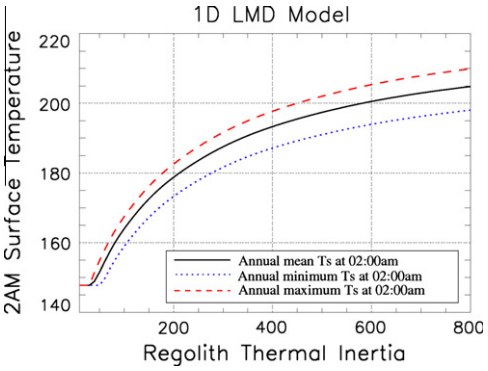

Fig. 9. Annual mean, maximum and minimum values of surface temperature (K) at local time 02:00 as a function of thermal inertia ($\text{J m}^{-2}\ \text{s}^{-1/2}\ \text{K}^{-1}$). Values are computed through single-column modeling sharing similar schemes for radiative transfer, soil energy budget, boundary-layer mixing as mesoscale simulations with the Spiga and Forget (2009) model. Latitude and pressure are set to the mean value for Olympus Mons.

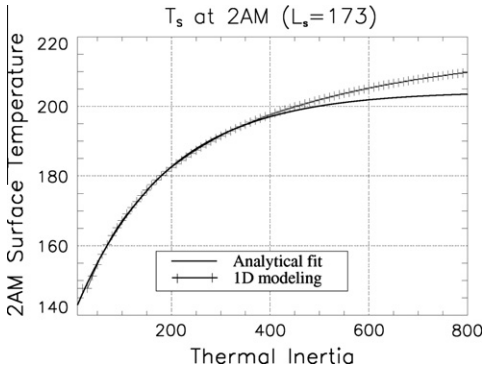

Fig. 10. Surface temperature (K) as a function of thermal inertia ($\text{J m}^{-2}\ \text{s}^{-1/2}\ \text{K}^{-1}$) as in Fig. 9, except that only the season chosen for the mesoscale simulation described in Fig. 4 is considered. Results from single-column modeling are shown with crosses. The analytical function $T_s = a_0(a_1 - e^{-a_2 I})$ with $a_0 = 64.83$ K, $a_1 = 3.15$ and $a_2 = 5.45 \times 10^{-3}\ \text{J}^{-1}\ \text{m}^2\ \text{K}\ \text{s}^{1/2}$ used to fit those results in the range $I \leqslant 400\ \text{J m}^{-2}\ \text{K}^{-1}\ \text{s}^{-1/2}$ is shown in full line.

6. Regional variability: why Olympus Mons is only an example

6.1. General principles

Olympus Mons is characterized by high and steep slopes yielding intense nighttime katabatic events, hence clear-cut warm signatures of surface temperature. It is an obvious case to discuss the influence of mesoscale winds on surface temperature. Yet processes by which atmospheric motions warm the surface are general enough to lead to suspicions that other terrains are impacted. Surface warming over more moderate slopes in Lycus Sulci suggest this is the case.

[9] Conversely, sensible heat flux makes atmospheric temperature colder than it would have been under the only influence of adiabatic heating. Still the latter effect dominates, hence warmer atmosphere above Olympus slopes than above surrounding plains (see Fig. 7). Note also that adiabatic heating acts as a positive feedback for katabatic winds because it enhances nighttime temperature inversions in near-surface layers. On the contrary, surface warming acts as a negative feedback since it lowers those temperature inversions. As a result, katabatic winds are not much impacted by thermal changes they induce and remain in steady regime.

[10] Fig. 1 of Mellon et al. (2000) shows that albedo, surface pressure, dust opacity are second-order influences on surface temperature, hence we do not consider those in our discussions.

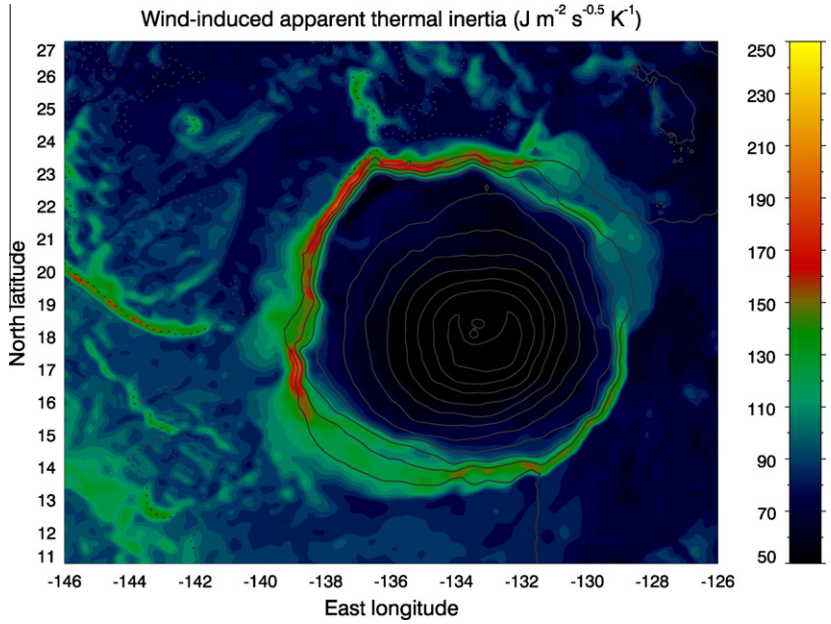

Fig. 11. "Wind-induced" nighttime apparent thermal inertia (J m^{-2} s$^{-1/2}$ K^{-1}) in the Olympus Mons/Lycus Sulci area, obtained by applying the function $I = f(T_s)$ determined in Fig. 10 to the surface temperature field predicted through mesoscale modeling in Fig. 4. Topography is contoured (contour interval is 2 km). Color scale is similar to Fig. 3 for the sake of comparison.

Are nighttime warm signatures on surface temperature widespread on Mars? Two factors may help to assess where temperature signatures and hence apparent thermal inertia variations are induced by atmospheric winds. Those two factors relate to the double effect of winds identified in Section 4.2:

1. The vertical component of katabatic winds must be large enough for adiabatic heating to be significant (cf. Eq. (2)). This is realized if the downslope acceleration is strong enough, which is the case for large near-surface temperature inversions $\Delta T/T$ and/or slope inclination α (according to the expression for slope buoyancy; Spiga (2011) Eq. (2)). The former contribution is not that different between slope and plain (see Fig. 7). The main constraint on adiabatic heating is thus associated with slope steepness. Slope length does not play a role as long as katabatic acceleration is strong enough to dominate friction, which is the case on Mars given large nighttime near-surface inversions $\Delta T/T$. Thus, the near-surface atmospheric warming predicted for Olympus Mons during the night will occur in virtually any location where the slope is steep enough. Olympus Mons is only one particularly extreme case.
2. The surface temperature must be significantly impacted by the atmospheric warming aloft. This is ensured by sensible heat flux being enhanced through horizontal component of katabatic circulations. However, Eq. (3) shows that any contribution to surface energy budget – radiative flux as well as sensible flux – would not impact significantly on surface temperature if thermal inertia is too high. In that case, heating/cooling contributions would take much more time to yield surface temperature changes. According to point (1), atmospheric warming by katabatic wind could appear over any steep slope, but this is not necessarily the case for surface warming. Signatures of surface temperature are mostly expected to appear clearly in low thermal inertia terrains (Olympus Mons is one of those). It can be seen in Fig. 9 that the lower the thermal inertia, the more steeply sloped is the function $T_s = f(I)$, meaning that a fixed departure in surface temperature would imply a larger difference in thermal inertia in low than in high thermal inertia terrains.

6.2. The example of Terra Meridiani

Phenomena identified over Olympus Mons could thus be found in terrains where topographical gradients are less extreme. This is exemplified by Terra Meridiani low-latitude cratered terrains. Compared to Olympus Mons, katabatic winds are less strong over Terra Meridiani where slopes are less steep; yet slopes are steep enough to allow katabatic winds to significantly warm the atmosphere. The effect is expected to be widespread over the Terra Meridiani plains composed of numerous craters with steep walls. In addition, average thermal inertia across Terra Meridiani is low enough for signatures to appear on the surface in the middle of the night. Fig. 12 shows mesoscale simulations[11] in Terra Meridiani assuming uniform (average) thermal inertia of 65 J m^{-2} K^{-1} s$^{-1/2}$. Katabatic winds are less prominent than over Olympus Mons terrains, yet still dominate nighttime mesoscale circulations in Meridiani terrains in the vicinity of crater slopes. Surface temperature departures caused by those circulations are significant (+10 to 15 K for moderately steep slopes). Here mesoscale simulations nicely illustrate the above-mentioned principle: slope steepness is a much more important control on katabatic intensity than slope length or scarp height. Surface temperature departures nearly as high as the ones predicted over Olympus Mons can also be found over a crater with steep enough slopes/rims. Discussions in the previous section about thermal inertia artifacts still hold for less extreme topographical obstacles than Olympus Mons. Fig. 12 shows that maps of retrieved thermal inertia in the Putzig and Mellon (2007a) dataset and of surface temperature in the mesoscale model simulations share similarities. Where surface temperature at local time 02:00 is predicted by the mesoscale model to be high, apparent thermal inertia is also high, especially in areas with sloping terrains. This correlation suggests similar thermal inertia artefacts in Terra Meridiani

[11] Nested simulations are employed to reach the fine horizontal resolution necessary to resolve topographical contrasts in Terra Meridiani. Results displayed in Fig. 12 are extracted from a simulation domain with horizontal resolution of 2.25 km "nested" within a larger simulation domain with horizontal resolution of 9 km, itself "nested" within a larger domain with horizontal resolution of 36 km. See Spiga and Forget (2009) for a detailed description of the grid nesting technique.

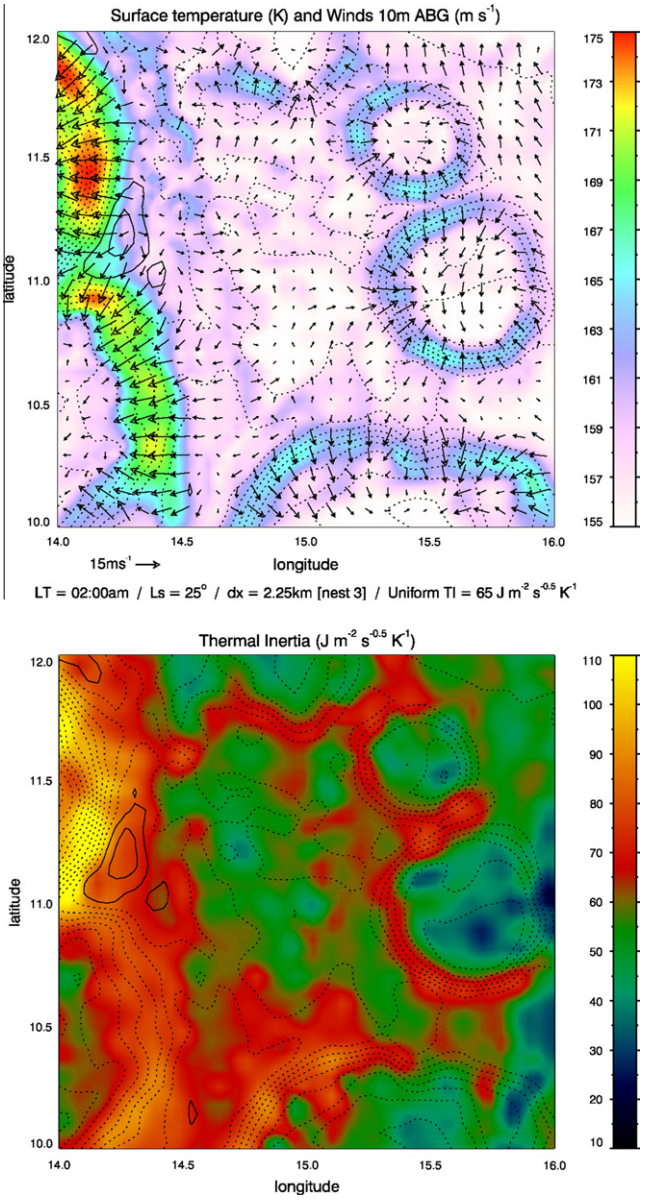

Fig. 12. (top) Surface temperature (K) and superimposed horizontal wind vectors 10 m above local surface ($m\,s^{-1}$) predicted in the Terra Meridiani region by a mesoscale simulation with 2.25 km horizontal resolution and uniform soil thermal inertia of 65 $J\,m^{-2}\,s^{-1/2}\,K^{-1}$ (season is northern spring, local time 02:00). Vectors are plotted for every other grid point. (bottom) Nighttime apparent thermal inertia ($J\,m^{-2}\,s^{-1/2}\,K^{-1}$) retrieved by Putzig and Mellon (2007a) from TES surface temperature measurements. Topography is contoured in both plots (contour interval is 250 m).

as the ones discussed in Olympus Mons. "Rings" of thermal inertia correlated with craters can also be distinguished all over Terra Meridiani and Arabia Terra on thermal inertia retrievals by Putzig and Mellon (2007a, their Fig. 8).

6.3. A new consistent atmospheric scenario that does not fully rule out the soil scenario

Discussions so far provide evidence that nighttime surface warming over slopes can be consistently accounted for by atmospheric winds only, which posits possible mismatches between apparent thermal inertia and intrinsic characteristics of the martian soil. Interestingly, we cannot rule out the possibility that apparent thermal inertia structures in sloping terrains could correspond to true thermal inertia signatures.

1. The impact of winds on surface temperature is all the more prominent over low thermal inertia terrains. In high thermal inertia terrains, katabatic winds also induce atmospheric heating and enhanced sensible heat flux, yet according to Eq. (3) surface temperature will not rise as rapidly as over low thermal inertia terrains (Figs. 4 and 12). This would be what could happen at the base of Olympus Mons if we assume that the high thermal inertia signatures of Fig. 3 exist. Indeed, mesoscale simulations featuring thermal inertia measured by Putzig and Mellon (2007a) instead of uniform value also replicate the contrasts of surface temperature observed by TES in Fig. 1. Predicted temperatures at the base of Olympus are only slightly warmer than in Fig. 4.
2. Katabatic winds over volcanoes and craters are persistent features of martian mesoscale meteorology in the night. These produce repetitive and intense aeolian (and, as we showed, thermal) erosion on martian soils. This could be a plausible reason for martian soils above which katabatic winds are blowing to differ those in surrounding plains. It is, however, not possible to determine either if winds could induce significant changes in soil thermophysical properties, or if these changes would be positive or negative.

Notwithstanding this, we showed that part of the surface temperature signal conveys information about slope winds. This has two important consequences.

1. Although our atmospheric scenario does not rule out the possibility that high thermal inertia signatures may exist in the vicinity of slopes in low thermal inertia terrains, it strengthens the Haberle and Jakosky (1991) statement: *We must caution against interpretation of the thermal inertia in terms of particle size without considering other relevant observations.* We demonstrated that it is not possible systematically to associate the spatial structures of apparent thermal inertia with soil properties because surface temperature is impacted by mesoscale circulations (notably katabatic winds over slopes). This issue must be ultimately addressed by a specific geological study.
2. If it is proven that signatures of apparent thermal inertia over a given slope cannot be related to contrasts of soil thermophysical properties, surface temperature maps (such as Fig. 1) would have great potential for martian atmospheric studies. In the context of paucity of observations, in particular the absence of quantitative near-surface wind speed data in martian sloping terrains, surface temperature can be used to help validate katabatic winds predicted through mesoscale modeling. The fact that surface temperature measured in the night by orbiting spacecraft could be predicted with good accuracy by the mesoscale model would indicate satisfactory predictions for nighttime katabatic winds. The double effect of mesoscale slope winds (especially the direct role of wind speed in surface warming) makes it likely that any significant error on evaluating the amplitude of those winds would in turn yield incorrect predictions for surface temperature.

7. Perspectives for daytime conditions and polar regions

In this section, we briefly mention two extensions of our discussions on nighttime wind-induced surface warming.

7.1. Afternoon surface cooling

Mechanisms by which atmospheric winds could warm the surface at night are general and apply to daytime conditions as well. Owing to temperature increase caused by Sun heating the surface in the afternoon, upslope (anabatic) winds develop on topographical

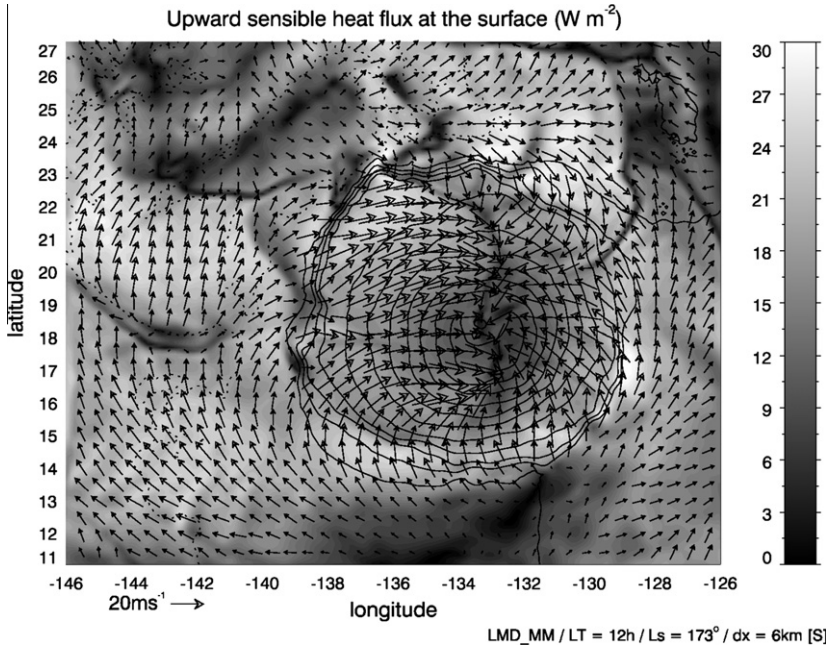

Fig. 13. Upward sensible heat flux (W m^{-2}) and superimposed horizontal wind vectors 10 m above local surface (m s^{-1}) predicted in the Olympus Mons/Lycus Sulci area at local time 12:00 by the mesoscale simulation described in Fig. 4. Topography is contoured (contour interval is 2 km). Vectors plotted every three grid points. This figure is the daytime counterpart of Fig. 8 bottom. Note that upward sensible heat flux corresponds to H_s according to the convention adopted in this paper: sensible heat exchanges act to cool the surface in the white areas of this figure.

obstacles (e.g. Spiga and Forget, 2009) which induce adiabatic expansion, hence atmospheric cooling (cf. Eq. (2) with positive sign for vertical velocity). Anabatic winds also act to reinforce sensible heat flux by enhancing horizontal wind and temperature difference between the surface and the atmosphere (Fig. 13). Heat is transferred more efficiently from the surface to the atmosphere, which is the exact opposite of nighttime conditions. Hence surface would be cooler than radiative equilibrium alone would indicate. Thus afternoon near-surface slope winds should induce surface cooling in the vicinity of martian slopes.

Interestingly, afternoon surface cooling has been observed (Palluconi and Kieffer, 1981; Ditteon, 1982) and remained to date unexplained, even considering the influence of airborne dust (Haberle and Jakosky, 1991). The impact of mesoscale winds on surface temperature is a new plausible scenario to account for those observations, where afternoon surface cooling is simply the daytime counterpart to surface warming caused by katabatic winds. This scenario could also explain high values of daytime apparent thermal inertia obtained by Putzig and Mellon (2007a, their Fig. 8) in the Olympus/Lycus and Terra Meridiani plains.[12] It is worthy of notice that, as shown in Fig. 13, upslope winds are not the strongest over the steepest flanks but over gently-sloping terrains,[13] which makes the latter more prone to afternoon cooling. Daytime conditions are however a bit more complex than nighttime conditions. An additional solar forcing term is added to the surface energy budget described by Eq. (3) with surface albedo, solar incidence angle and slope steepness being involved. The impact of wind-induced phenomena on surface temperature are more difficult to isolate in daytime than in nighttime; this would require calculations out of the scope of the present paper and left for future work. Nevertheless, the impact of mesoscale winds on surface temperature appears, at least qualitatively, as a robust scenario to account for observed afternoon surface cooling in moderately-sloped terrains.

7.2. The case of ice-covered slopes

This paper focusses on the impact of atmospheric winds on surface temperature. On a broader perspective, we showed that the martian atmosphere could play an important role, hitherto underestimated, in surface energy budget (cf. Eqs. (1) and (3)). This can be further illustrated by discussing implications of our findings for ice-covered slopes, notably in polar regions.

Fig. 14 shows results from a dedicated 10 km-resolution mesoscale simulation at $L_s = 61^\circ$ with a stereographic projection domain centered on the northern polar cap. The predicted directions for near-surface winds over martian northern cap are governed by an equilibrium between katabatic acceleration, Coriolis deflection and surface friction, in line with wind streak mapping (Howard, 2000). The presence of ice on sloping terrains reinforces near-surface temperature inversions hence katabatic acceleration (e.g. Doran et al., 1990, 2001, 2008). In conditions of CO_2 frost cover, which is the case in the whole area displayed in Fig. 14, strong downslope winds persist for the whole day. Thus martian polar caps would be prone to the mesoscale wind-induced impact described in this paper. An enhancement of downward sensible heat flux $-H_s$ caused by katabatic winds, which can transfer to the surface atmospheric heating caused by those same winds, is indeed predicted by mesoscale simulations in Fig. 14. Sensible heat flux is especially enhanced above the troughs with the steepest slopes. Contrary to lower-latitude terrains, in winter polar regions this increase in sensible flux would not force the surface temperature to rise above the CO_2 solid/gas phase equilibrium. Instead, it would modify the condensation/sublimation rate of CO_2 surface frost. Sensible heat transferred to the surface through katabatic winds would be consumed through latent heat to sublimate CO_2 frost and maintain the surface temperature at its fixed (surface pressure dependent) phase transition value. This can be illustrated by the modified Eq. (3)

[12] Similarly to nighttime conditions, possible departures of surface temperature caused by daytime winds would be more prominent in regions of low thermal inertia.

[13] Slope must be steep enough for slope acceleration to be significant, but not too steep to optimize exposure to incoming sunlight. This is not the case for katabatic winds for which slope steepness is the main control (friction apart) for wind speed.

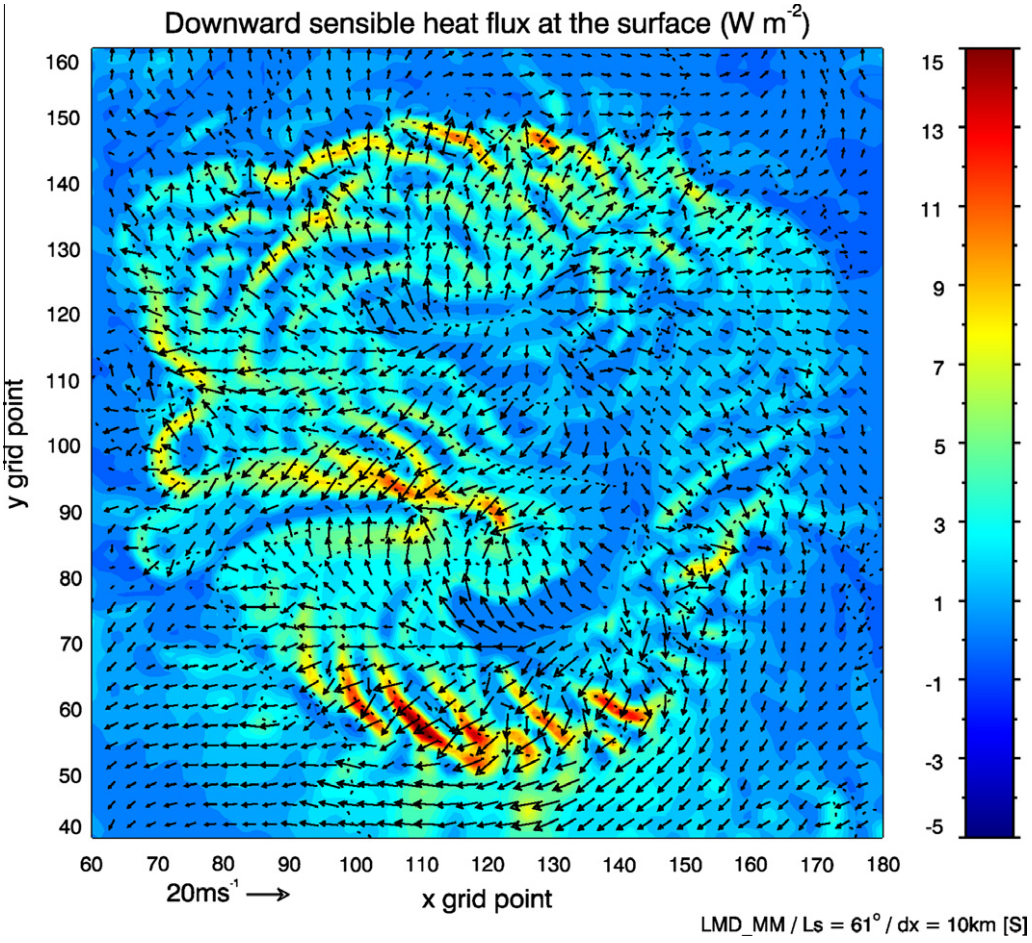

Fig. 14. Downward sensible heat flux (W m^{-2}) and superimposed horizontal wind vectors 10 m above local surface (m s^{-1}) predicted in the northern polar region by a mesoscale simulation with 10 km horizontal resolution and polar stereographic projection. Season is northern spring, universal time 09:00. Topography is contoured (contour interval is 1 km). Vectors each three grid points. Note that downward sensible heat flux corresponds to $-H_s$ according to the convention adopted in this paper: sensible heat exchanges act to warm the surface in yellow/red areas of this figure.

$$\epsilon\sigma T_s^4 = I\sqrt{\frac{\pi}{\tau}}\frac{\partial T_g}{\partial \zeta}\Big|_{\zeta=0} + \mathcal{F}_{IR} - H_s + L\frac{\partial M}{\partial t} \quad (4)$$

where L is the latent heat of CO_2 sublimation and M the mass of CO_2 frost and t time.

Sensible heat flux can reach 18 W m^{-2} over the steepest slopes in our mesoscale simulations. Hence the variations of the mass of CO_2 frost with time in those regions can be significantly impacted since radiative flux $\epsilon\sigma T_s^4$ is only 23 W m^{-2} when T_s = 145 K and ϵ = 0.9 (typical values for ground CO_2 ice). Katabatic winds tend to increase CO_2 sublimation rate in spring and limit CO_2 condensation in winter. The steeper the slope the less stable the CO_2 ice deposits would be. Thus, our discussions on the thermal impact of mesoscale winds on the surface provide new constraints on the stability of CO_2 ices in martian polar caps, and more generally over any martian sloping terrains (see Vincendon et al. (2010) and references therein).

Recent conclusions by Holt et al. (2010) and Smith and Holt (2010) based on radar stratigraphy has renewed early arguments in favor of wind transport and atmospheric deposition as crucial processes for shaping martian polar caps (including spiral pattern, see also Ng and Zuber, 2006). We can wonder if the thermal impact of katabatic winds might have played a role in those processes. In particular, is it possible that slope winds developing over an existing polar trough could enhance sublimation rate, thereby deepening this existing trough and implying a positive feedback for trough formation in the martian polar caps? It remains to be determined though how H_2O ice deposits would react to katabatic wind warming given that, contrary to CO_2 ice, their temperature can rise and their condensation/sublimation rate is controlled by partial vapor pressure and the amount of precipitation. A detailed modeling study of those key issues is considered as future work.

8. Conclusions

According to nighttime TES measurements in various non-dusty seasons, the martian surface is up to +20 K warmer on slopes than on surrounding plains in the Olympus Mons/Lycus Sulci region. Thus far, it has been thought that such behavior was due to contrasts in soil thermophysical properties, especially thermal inertia. We show through mesoscale modeling that those warm surface departures in the night, correlated with slope steepness, could just as well be accounted for by mesoscale atmospheric winds only.

Radiative cooling causes powerful katabatic winds to form over martian sloping terrains all night long in various seasons. Those mesoscale downslope circulations have a twofold thermal impact on the martian atmosphere and surface:

1. Their vertical component results in adiabatic compression and heating of the atmosphere, which could overwhelm infrared radiative cooling and only be balanced by the equally strong turbulent cooling described in (2).
2. Their horizontal component enhances the downward sensible heat flux, thereby allowing the warmer atmosphere described in (1) to heat the surface.

The impact of mesoscale winds on surface temperature is particularly prominent over steep slopes in low thermal inertia terrains. Olympus Mons is only an extreme example amongst others: for instance, observations and mesoscale modeling indicate that Terra Meridiani cratered terrains are prone to the same phenomenon as Olympus terrains.

Thus, despite the low density of the martian atmosphere, sensible heat flux cannot be systematically neglected in surface energy budget: over martian slopes in the night, it might become comparable to longwave radiative loss. We conclude that surface radiative equilibrium does not hold everywhere on Mars, contrary to a common assumption. We show that neglecting the contribution of martian atmospheric winds in the surface energy budget could have adversely affected thermal inertia retrievals to the point that artificial (wind-induced) structures correlated with slopes would appear in apparent thermal inertia field. Warm signatures of surface temperature over slopes in orbital infrared measurements cannot be systematically associated with contrasts of intrinsic characteristics of martian soil. Part of the surface temperature signal conveys information about slope winds. This makes surface temperature maps in uneven terrains of great potential value to validate katabatic wind speeds predicted through mesoscale modeling, provided systematic thermal inertia contrasts can be ruled out through geological analysis.

We showed that katabatic winds can have a strong thermal impact, in addition to their well-known aeolian influence. Mechanisms by which atmospheric winds warm the surface at night could also apply to

- daytime conditions: this could account for the still unexplained observations of afternoon surface cooling over moderately-sloped terrains;
- ice-covered regions: the thermal impact of winds would not cause surface temperature to rise, but sublimation rate to increase, which could have an influence on ice stability.

Our conclusions offer the possibility of improved future thermal inertia retrievals, more unambiguously representing intrinsic characteristics of martian soil. For instance, the identified correlation between surface katabatic warming and slope steepness, if robust enough, could be used to find parameterizations for the sensible heat term in Eq. (3) describing surface energy budget.

This work exemplifies how studying the martian atmospheric circulation, through observations or modeling, results in constraints not only on the meteorology but also on the geology of Mars. This is one of the reason why sending instruments probing the martian winds on board upcoming missions should still be considered as a priority. The martian surface and atmosphere are more coupled than hitherto thought.

Acknowledgments

We would like to express our gratitude to Tim Michaels and Hannu Savijärvi for rigorous reviews and insightful comments which improved the paper. We acknowledge support from European Space Agency (ESTEC TRP Contract 11369) and Centre National d'Etudes Spatiales.

Appendix A. Formula for sensible heat flux in nighttime stable conditions

In this brief appendix, we discuss the validity in nighttime stable conditions of the bulk formula for sensible heat flux $H_s = \rho c_p \sqrt{C_d} u_* T_*$. Friction velocity u_* is the product between horizontal wind speed $V(z_1)$ and the square root of the von Karman drag coefficient $C_d = [0.4/\ln(z_1/z_0)]^2$ (z_0 is the surface roughness). Strictly speaking, the denominator in the equation for C_d is $\ln(z_1/z_0)$ only in neutral conditions. In stable conditions, it should be $\ln(z_1/z_0) - \Psi(Ri_b)$, where Ψ is a stability function of the bulk Richardon parameter $Ri_b = gT_*/[\langle T \rangle V(z_1)^2]$, negative for unstable conditions (Mahrt, 2008; Garratt, 1992, Section 3.3.2). However, values in Fig. 7 above Olympus Mons slopes yield $Ri_b \sim 10^{-4}$ hence C_d being reasonably close to neutral formulation (Mahrt, 2008, his Figs. 2 and 3).

Another way to consider this issue is to calculate Obukhov length L which relates stability and wind shear in the surface layer (Garratt, 1992). The ratio of L between Olympus slopes and surrounding plains is approximatively equal to the ratio of u_*^2 between the two sites, ~300 according to values in Fig. 7. In martian plains, L was measured to be close to 3 m in nighttime conditions (Sutton et al., 1978), hence $L \sim 10^3$ m over Olympus Mons slopes, hence $z/L \sim 10^{-2}$ at altitude 10 m above the surface (here Monin–Obukhov similarity can be used because the depth of slope flow layer is comparable to L, see Grisogono et al., 2007). Variations of the stability function $-\Psi$ with z/L are approximatively linear, and $-\Psi \ll 1$ for $z/L \sim 10^{-2}$ (Mahrt, 2008, his Fig. 1), hence $-\Psi(Ri_b) \ll \ln(z_1/z_0)$ and $C_d \simeq [0.4/\ln(z_1/z_0)]^2$.

Thus, it appears that it is a good approximation to use the simple neutral bulk formulation for sensible heat flux so as to represent surface–atmosphere interactions in situation of strong stationary katabatic flow in stable conditions. Difficulties only arise for weak-wind conditions in highly stable surface layers. This was confirmed by comparisons of observed and parameterized near-surface turbulent heat fluxes, which showed good agreement for low bulk Richardson numbers (e.g., observations in Antarctica by Cassano et al. (2001)).

References

Bandfield, J.L., Feldman, W.C., 2008. Martian high latitude permafrost depth and surface cover thermal inertia distributions. J. Geophys. Res. (Planets) 113, E08001.

Basilevsky, A.T., Werner, S.C., Neukum, G., Head, J.W., van Gasselt, S., Gwinner, K., Ivanov, B.A., 2006. Geologically recent tectonic, volcanic and fluvial activity on the eastern flank of the Olympus Mons volcano, Mars. Geophys. Res. Lett. 33, L13201.

Bleacher, J.E., Greeley, R., Williams, D.A., Werner, S.C., Hauber, E., Neukum, G., 2007. Olympus Mons, Mars: Inferred changes in late Amazonian aged effusive activity from lava flow mapping of Mars Express High Resolution Stereo Camera data. J. Geophys. Res. (Planets) 112, E04003.

Brack, A., 1996. Why exobiology on Mars? Planet. Space Sci. 44, 1435–1440.

Bromwich, D.H., Cassano, J.J., Klein, T., Heinemann, G., Hines, K.M., Steffen, K., Box, J.E., 2001. Mesoscale modeling of katabatic winds over greenland with the polar MM5. Mon. Weather Rev. 129, 2290–2309.

Cassano, J.J., Parish, T.R., King, J.C., 2001. Evaluation of turbulent surface flux parameterizations for the stable surface layer over Halley, Antarctica. Mon. Weather Rev. 129, 26–46.

Christensen, P.R. et al., 2001. Mars Global Surveyor Thermal Emission Spectrometer experiment: Investigation description and surface science results. J. Geophys. Res. 111, 23823–23872.

Clancy, R.T., Sandor, B.J., Woff, M.J., Christensen, P.R., Smith, M.D., Pearl, J.C., Conrath, B.J., Wilson, R.J., 2000. An intercomparison of ground-based millimeter, MGS TES, and Viking atmospheric temperature measurements: Seasonal and interannual variability of temperatures and dust loading in the global Mars atmosphere. J. Geophys. Res. 105, 9553–9571.

Ditteon, R., 1982. Daily temperature variations on Mars. J. Geophys. Res. 87, 10197–10214.

Doran, J.C., Horst, T.W., Whiteman, C.D., 1990. The development and structure of nocturnal slope winds in a simple valley. Boundary-Layer Meteorol. 52, 41–68.

Fergason, R.L., Christensen, P.R., Bell, J.F., Golombek, M.P., Herkenhoff, K.E., Kieffer, H.H., 2006. Physical properties of the Mars Exploration Rover landing sites as inferred from Mini-TES-derived thermal inertia. J. Geophys. Res. (Planets) 111, E02S21.

Forget, F., Hourdin, F., Fournier, R., Hourdin, C., Talagrand, O., Collins, M., Lewis, S.R., Read, P.L., Huot., J.-P., 1999. Improved general circulation models of the martian atmosphere from the surface to above 80 km. J. Geophys. Res. 104, 24155–24176.

Garratt, J.R., 1992. The Atmospheric Boundary Layer. Cambridge Univ. Press, New York.

Greeley, R., Kuzmin, R.O., Rafkin, S.C.R., Michaels, T.I., Haberle, R., 2003. Wind-related features in Gusev crater, Mars. J. Geophys. Res. (Planets) 108 (E12), 8077.
Grisogono, B., Kraljević, L., Jeričević, A., 2007. The low-level katabatic jet height versus Monin–Obukhov height. Q. J. R. Meteorol. Soc. 133 (629), 2133–2136.
Haberle, R.M., Jakosky, B.M., 1991. Atmospheric effects on the remote determination of thermal inertia of Mars. Icarus 90, 187–204.
Holt, J.W., Fishbaugh, K.E., Byrne, S., Christian, S., Tanaka, K., Russell, P.S., Herkenhoff, K.E., Safaeinili, A., Putzig, N.E., Phillips, R.J., 2010. The construction of Chasma Boreale on Mars. Nature 465, 446–449.
Hourdin, F., Le Van, P., Forget, F., Talagrand, O., 1993. Meteorological variability and the annual surface pressure cycle on Mars. J. Atmos. Sci. 50, 3625–3640.
Howard, A.D., 2000. The role of eolian processes in forming surface features of the martian polar layered deposits. Icarus 144, 267–288.
Hynek, B.M., Singer, K., 2007. Ground truth from the Opportunity Rover for Mars thermal inertia data. Geophys. Res. Lett. 34, L11201.
Jakosky, B.M., Mellon, M.T., Kieffer, H.H., Christensen, P.R., Varnes, E.S., Lee, S.W., 2000. The thermal inertia of Mars from the Mars Global Surveyor Thermal Emission Spectrometer. J. Geophys. Res. 105, 9643–9652.
Jouglet, D., Poulet, F., Langevin, Y., Bibring, J., Gondet, B., Vincendon, M., Berthe, M., 2009. OMEGA long wavelength channel: Data reduction during non-nominal stages. Planet. Space Sci. 57, 1032–1042.
Kauhanen, J., Siili, T., Järvenoja, S., Savijärvi, H., 2008. The Mars limited area model and simulations of atmospheric circulations for the Phoenix landing area and season of operation. J. Geophys. Res. (Planets) 113, E00A14.
Kieffer, H.H., Chase, S.C., Miner, E.D., Palluconi, F.D., Münch, G., Neugebauer, G., Martin, T.Z., 1976. Infrared thermal mapping of the martian surface and atmosphere: First results. Science 193, 780–786.
Kieffer, H.H., Martin, T.Z., Peterfreund, R., Jakosky, B.M., Miner, E.D., Palluconi, F.D., 1977. Thermal and albedo mapping during the Viking primary mission. J. Geophys. Res. 82, 4249–4291.
Lewis, S.R., Barker, P.R., 2005. Atmospheric tides in a Mars general circulation model with data assimilation. Adv. Space Res. 36, 2162–2168.
Mahrt, L., 1982. Momentum balance of gravity flows. J. Atmos. Sci. 39 (12), 2701–2711.
Mahrt, L., 2008. Bulk formulation of surface fluxes extended to weak-wind stable conditions. Q. J. R. Meteorol. Soc. 134 (630), 1–10.
McGovern, P., Morgan, J., 2009. Volcanic spreading and lateral variations in the structure of Olympus Mons, Mars. Geology 37 (2), 139–142.
Mellon, M.T., Jakosky, B.M., Kieffer, H.H., Christensen, P.R., 2000. High resolution thermal inertia mapping from the Mars Global Surveyor Thermal Emission Spectrometer. Icarus 148, 437–455.
Michaels, T.I., Colaprete, A., Rafkin, S.C.R., 2006. Significant vertical water transport by mountain-induced circulations on Mars. Geophys. Res. Lett. 33, L16201.
Millour, E., Forget, F., Lewis, S.R., 2008. Mars Climate Database v4.3 Detailed Design Document, Technical Note ESTEC Contract 11369/95/NL/JG.
Ng, F.S.L., Zuber, M.T., 2006. Patterning instability on the Mars polar ice caps. J. Geophys. Res. (Planets) 111, E02005.
Nylen, T.H., Fountain, A.G., Doran, P.T., 2004. Climatology of katabatic winds in the McMurdo dry valleys, southern Victoria Land, Antarctica. J. Geophys. Res. (Atmos.) 109, D03114.
Palluconi, F.D., Kieffer, H.H., 1981. Thermal inertia mapping of Mars from 60°S to 60°N. Icarus 45, 415–426.
Presley, M., Christensen, P., 1997. The effect of bulk density and particle size sorting on the thermal conductivity of particulate materials under martian atmospheric pressures. J. Geophys. Res. 102 (E4), 9221–9229.
Putzig, N.E., Mellon, M.T., 2007a. Apparent thermal inertia and the surface heterogeneity of Mars. Icarus 191, 68–94.
Putzig, N.E., Mellon, M.T., 2007b. Thermal behavior of horizontally mixed surfaces on Mars. Icarus 191, 52–67.
Putzig, N.E., Mellon, M.T., Kretke, K.A., Arvidson, R.E., 2005. Global thermal inertia and surface properties of Mars from the MGS mapping mission. Icarus 173, 325–341.
Rafkin, S.C.R., Haberle, R.M., Michaels, T.I., 2001. The Mars regional atmospheric modeling system: Model description and selected simulations. Icarus 151, 228–256.
Rafkin, S.C.R., Michaels, T.I., 2003. Meteorological predictions for 2003 Mars Exploration Rover high-priority landing sites. J. Geophys. Res. (Planets) 108 (E12), 8091.
Rafkin, S.C.R., Sta. Maria, M.R.V., Michaels, T.I., 2002. Simulation of the atmospheric thermal circulation of a martian volcano using a mesoscale numerical model. Nature 419, 697–699.
Savijärvi, H., Kauhanen, J., 2008. Surface and boundary-layer modelling for the Mars Exploration Rover sites. Q. J. R. Meteorol. Soc. 134, 635–641.
Savijärvi, H., Määttänen, A., 2010. Boundary-layer simulations for the Mars Phoenix lander site. Q. J. R. Meteorol. Soc. 136, 1497–1505.
Savijärvi, H., Määttänen, A., Kauhanen, J., Harri, A.-M., 2004. Mars Pathfinder: New data and new model simulations. Q. J. R. Meteorol. Soc. 130, 669–683.
Savijärvi, H., Siili, T., 1993. The martian slope wind and the nocturnal PBL jet. J. Atmos. Sci. 50, 77–88.
Skamarock, W.C., Klemp, J.B., 2008. A time-split nonhydrostatic atmospheric model for weather research and forecasting applications. J. Comput. Phys. 227, 3465–3485.
Smith, I.B., Holt, J.W., 2010. Onset and migration of spiral troughs on Mars revealed by orbital radar. Nature 465, 450–453.
Smith, M.D., Pearl, J.C., Conrath, B.J., Christensen, P.R., 2001. Thermal emission spectrometer results: Mars atmospheric thermal structure and aerosol distribution. J. Geophys. Res. 106, 23929–23945.
Spiga, A., 2011. Elements of comparison between martian and terrestrial mesoscale meteorological phenomena: Katabatic winds and boundary layer convection. Planet. Space Sci., in press.
Spiga, A., Forget, F., 2008. Fast and accurate estimation of solar irradiance on martian slopes. Geophys. Res. Lett. 35, L15201.
Spiga, A., Forget, F., 2009. A new model to simulate the martian mesoscale and microscale atmospheric circulation: Validation and first results. J. Geophys. Res. (Planets) 114, E02009.
Spiga, A., Forget, F., Lewis, S.R., Hinson, D.P., 2010. Structure and dynamics of the convective boundary layer on Mars as inferred from large-eddy simulations and remote-sensing measurements. Q. J. R. Meteorol. Soc. 136, 414–428.
Spiga, A., Lewis, S.R., Forget, F., Millour, E., Montabone, L., Madeleine, J., 2010. The impact of katabatic winds on martian thermal inertia retrievals. In: Lunar and Planetary Institute Science Conference Abstracts, vol. 41. Technical Report, p. 1533.
Sutton, J.L., Leovy, C.B., Tillman, J.E., 1978. Diurnal variations of the martian surface layer meteorological parameters during the first 45 sols at two Viking lander sites. J. Atmos. Sci. 35, 2346–2355.
Toigo, A.D., Richardson, M.I., 2002. A mesoscale model for the martian atmosphere. J. Geophys. Res. (Planets) 107 (E12), 5049.
Tyler, D., Barnes, J.R., Haberle, R.M., 2002. Simulation of surface meteorology at the Pathfinder and VL1 sites using a Mars mesoscale model. J. Geophys. Res. (Planets) 107 (E4), 5018.
Vincendon, M., Mustard, J., Forget, F., Kreslavsky, M., Spiga, A., Murchie, S., Bibring, J., 2010. Near-tropical subsurface ice on Mars. Geophys. Res. Lett. 37, L01202.
Wolkenberg, P., Formisano, V., Rinaldi, G., Geminale, A., 2010. The atmospheric temperatures over Olympus Mons on Mars: An atmospheric hot ring. Icarus 207, 110–123.
Ye, Z.J., Segal, M., Pielke, R.A., 1990. A comparative study of daytime thermally induced upslope flow on Mars and Earth. J. Atmos. Sci. 47, 612–628.